PCCP

PAPER

View Article Online
View Journal | View Issue

Cite this: *Phys. Chem. Chem. Phys.*, 2023, **25**, 31726

Effect of copper doping on plasmonic nanofilms for high performance photovoltaic energy applications

Ghulam Hasnain Tariq,[a] Ghulam Asghar,[b] M. Shahzad Shifa,[c] M. Anis-Ur-Rehman,[d] Sana Ullah,[e] Zulfiqar Ali Shah,[f] Imane Ziani,[gh] Ahmed M. Tawfeek[i] and Farooq Sher *[j]

In the current era, alternative but environment-friendly sources of energy have gained attention to meet the growing energy demands. In particular, the focus of research has been solar energy and using it to fulfill energy demands. Solar energy is either directly converted into electrical energy or stored for later use. Solar cells are a practical way to turn solar energy into electrical energy. Various materials are being investigated to manufacture solar cell devices that can absorb a maximum number of photons present in sunlight. The present study reports thermally evaporated *in situ* Cu-doped SnS photon absorber thin films with tunable physical properties. This study mainly explored the effects of changing Cu concentrations on the physical features of light absorption of SnS thin films. The thin films were formed by simultaneous resistive heating of Cu and SnS powders on glass substrates at 150 °C. The X-ray diffraction patterns revealed pure SnS thin films having orthorhombic polycrystalline crystal structures oriented preferentially along the (111) plane. Raman spectroscopy confirmed this phase purity. Photoconductivity studies showed phase dependence on Cu content that improved with increasing concentrations of Cu. The optical bandgap energy was also found to be dependent on Cu content and was observed at 1.10–1.47 eV for SnS thin films with variation in the Cu content, *i.e.*, 0–18%. According to the hot probe method, all films displayed p-type conductivity for the substitution of Cu metal atoms. These findings demonstrated that the prepared thin films are substantial candidates as low-cost, suitably efficient, thin-film solar cells featuring environmentally-friendly active layers that absorb sunlight.

Received 6th September 2023,
Accepted 3rd November 2023

DOI: 10.1039/d3cp04332k

rsc.li/pccp

1. Introduction

Recent researches have been focused mainly on low-cost, non-toxic and eco-friendly semiconducting materials, particularly the graphene/hydroxyapatite nano-composite,[1] with direct relevance to solar energy applications. As the world increasingly shifts towards cleaner and more sustainable energy sources, the critical role of solar energy becomes evident. Within solar energy systems, the need for efficient energy storage and conversion methods is paramount. However, hydrogen is celebrated for its clean and renewable nature that holds great potential. Enhancing hydrogen production through innovative nano-composites advocates for a holistic and environmentally conscious approach to address global energy demands and enhance the feasibility of solar energy integration. In a similar vein, recent research on B-/N-codoped graphene quantum dots (GQDs) provides valuable insights into optimizing materials for various solar energy applications,[2] laying the foundation for potential improvements in material design and optimization, ultimately enhancing the efficiency of solar cells employing diverse semiconductor materials.

[a] *Institute of Physics, Khwaja Fareed University of Engineering and Information Technology, Rahim Yar Khan 64200, Pakistan*
[b] *Department of Physics, The University of Poonch, Rawalakot 10250, Pakistan*
[c] *Institute of Physics, Islamia University Bahawalpur, Bahawalpur 63100, Pakistan*
[d] *Applied Thermal Physics Laboratory, Department of Physics, COMSATS University Islamabad, Islamabad, Pakistan*
[e] *Institute of Mechanical and Manufacturing Engineering, Khwaja Fareed University of Engineering and Information Technology, Rahim Yar Khan 64200, Pakistan*
[f] *Department of Physics, Allama Iqbal Open University, Islamabad, Pakistan*
[g] *Physical Chemistry of Natural Substances and Process Research Team, Laboratory of Applied Chemistry and Environment (LCAE-CPSUNAP), Faculty of Sciences, Mohammed 1st University, Oujda 60000, Morocco*
[h] *International Society of Engineering Science and Technology, Nottingham, UK*
[i] *Department of Chemistry, College of Science, King Saud University, P.O. Box 2455, Riyadh 11451, Saudi Arabia*
[j] *Department of Engineering, School of Science and Technology, Nottingham Trent University, Nottingham NG11 8NS, UK. E-mail: Farooq.Sher@ntu.ac.uk; Tel: +44 (0)115 84 86679*

When it comes to thin-film solar cells, the trend is to discover an active and effective photon absorber layer. Tin sulfide (SnS) is a chalcogenide semiconductor binary compound consisting of group IV–VI earth-abundant nonpoisonous elemental materials tin (Sn) and sulfur (S). Tin sulfide (SnS) is a chalcogenide semiconductor binary compound consisting of group IV–VI earth-abundant nonpoisonous elemental materials Tin (Sn) and sulfur (S). P-type semiconductors include SnS[3] and have a band gap[4] of 1 to 1.57 eV,[5] sometimes close to that of Si.[6] Because of this optimum gap, the SnS absorber layer is used not only as an alternative for photovoltaic applications but also for gas sensing applications.[7] With varying bandgaps,[8] un-doped and doped SnS[9] has an elevated absorption coefficient[10] of about 10^4 cm^{-1} and has a suitable theoretical energy conversion efficiency[11] of $>25\%$.[12]

Although SnS thin-film solar cells have not reached their theoretical energy conversion efficiency, they have achieved a record efficiency of 44.36%.[13] This difference prompts a fascination to discover synthesis methods for more efficient SnS thin films and to explore their physical properties for credible light absorbent layers for solar cells. Different physical properties like morphology, crystallinity, charge carrier nature and band gap energy have a considerable influence on the performance of SnS thin film solar cells. Moreover, the junction properties present at the heterojunction affect the performance and efficiency of SnS thin film solar cells (TFSCs). The stresses present at the heterojunction impede transport within and across the junction[14] and produce interface recombination[15] that reduces the efficiency of SnS solar cells.[9] To overcome these limitations, doping is used in most semiconductor materials. Different extrinsic doping elements have been investigated to enhance the physical characteristics, like energy band gap, photoconductivity, *etc.*, and to produce desired electrical characteristics. These band gap modifications with external dopants affect the discontinuities of both the valence and conduction bands. Substitutional external doping at Sn sites within the SnS crystal lattice makes modifications in the acceptor densities, which further improve the solar cell performance and efficiency.[16] Optimization of external dopants' nature and concentration of external dopants is essential to achieve the appropriate acceptance density of SnS thin films.

Different dopants incorporated in SnS thin films including silver,[16] silver by sputtering,[17] and spray pyrolysis,[18] aluminum,[19] nickel,[20] indium-doped thin films[21] and nanoparticles,[10] chlorine,[22] and copper-doped by spray pyrolysis[23] and electrodeposited[24] have modified the physical features of SnS thin films significantly. Cu-doped CdTe,[25] Zn-doped CdS,[26] Bi-doped CdTe,[27] and Al dope ZnS[28] are some different examples of doping of binary compounds. Among these elements, copper is a potential dopant that can enhance the collection of charge carriers and stabilize the Fermi level in different semiconductor thin film materials. Therefore, the present research work comprises an inclusive study of the effects of Cu doping on the physical features of SnS thin films for light-absorbing layers in photovoltaic applications.

Numerous deposition methods have been applied to prepare doped SnS thin films, which include deposition in a chemical bath,[29] spin coating,[30] spray pyrolysis,[18] thermal evaporation,[29] *etc.* The solution-based synthesis of SnS thin films involves the preparation of two distinct precursors, known as precursor A and precursor B.[31] These precursors are created by dissolving tin(II) 2-ethylhexanoate and tin(II) chloride dihydrate in appropriate solvents, respectively. Additional chemicals, such as glacial acetic acid, thiourea, triethanolamine, and ethanolamine, are added to these precursors. After 24 hours of gentle stirring at room temperature, transparent and uniform solutions are obtained. Subsequently, thin films are fabricated by dip-coating substrates in these solutions and subjecting them to a vertical furnace. Regarding carrier type, SnS thin films produced using tin(II) 2-ethylhexanoate as the starting chemical exhibit p-type conductivity, while films prepared with tin(II) chloride dihydrate as the starting chemical demonstrate n-type conductivity under specific Sn/S ratios. P-type films have an electrical resistivity on the order of 10^6 Ω cm, whereas n-type films exhibit a resistivity of around 10^1 Ω cm.[31]

The development of inexpensive deposition of thin films is the most investigated part of the photovoltaic research field. Therefore, the present study systematically investigates the effect of Cu doping on the optical, photoconductive, and structural properties of orthorhombic SnS thin films using vacuum thermal evaporation as the oldest and simplest method of deposition of thin films. For the first time, the effect of *in situ* Cu doping on the physical properties of SnS thin films deposited by co-evaporation of Cu and SnS under vacuum is reported in this study. This investigation into the effects of *in situ* Cu doping on the SnS thin films' physical characteristics will be useful in determining the best synthesis conditions to achieve the physical properties needed to capture the majority of the solar spectrum.

2. Experimental

2.1 Synthesis of Cu-doped SnS thin films

Cu-doped SnS thin films with a thickness of approximately 300 nm were deposited onto soda lime silicate glass substrates measuring 75 × 25 mm. The deposition process involved simultaneous thermal evaporation of Cu and SnS powder precursors using an Alumnia crucible and a Molybdenum boat, respectively. To ensure uniform thickness, the glass substrates were placed on a substrate holder directly above the sources and clamped securely with a spring-loaded strip (Fig. 1). A crucial factor in achieving uniform thickness was maintaining a consistent source-to-substrate distance, which was set at 21 cm for all depositions. This distance is significant as the thin film deposition rate follows the Knudsen cosine rule.[32] The deposition rate is proportional to the ratio $(\cos\theta/r^2)$, where 'r' represents the radial separation from the source to the substrate's deposition point, and 'θ' denotes the angle formed by 'r' and the source's normal in the direction of the substrate. Additionally, the condition of the substrate's surface significantly influences the thin film structure and uniform deposition. Before deposition, all substrates underwent thorough

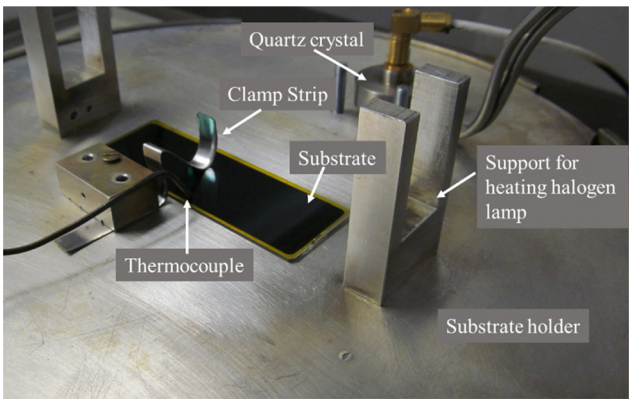

Fig. 1 Adjustment of the substrate, thermocouple, heating halogen lamp and quartz crystal on the substrate holder.

cleaning using a well-designed scheme to ensure the best possible surface conditions.[33]

2.2 Post-deposition processing and Cu doping

Following the deposition process, the deposition rate was kept at 8.7 Å s^{-1} and thin films reached a thickness of 1 μm. The film thickness was monitored using a quartz crystal thickness monitor attached near the substrate (Fig. 1). A thermocouple was directly attached to the substrate to measure its temperature during deposition. The deposition occurred in a base vacuum of 2×10^{-6} mbar, created using a combination of an oil diffusion pump equipped with a liquid nitrogen trap and a rotary mechanical vacuum pump. Throughout the deposition, the vacuum was maintained in the range of 8×10^{-6} to 2×10^{-5} mbar. All substrates were kept at 150 °C by a halogen lamp placed directly above the substrate in the support shown in Fig. 1. After deposition, the samples were left at the same temperature (150 °C) for 20 minutes to cool down to room temperature. The Cu doping percentage varied from 0 to 18%, as detailed in Table 1. To enhance dopant diffusion and improve the physical properties,[34] all the prepared samples underwent a one-hour vacuum annealing process at 350 °C.[35] For this process, the thin films were placed in evacuated Pyrex glass tubes, sealed at a pressure of about 10^{-2} torr, and heated in a furnace. This vacuum annealing step was essential for optimizing dopant diffusion and achieving the desired physical properties in the Cu-doped SnS thin films.

2.3 Material composition and structure analysis

Cu-doped SnS thin films underwent a thorough analysis to uncover their material composition and structural properties, essential for their application in photovoltaics, particularly in thin film solar cell devices.[36] The analysis began with the use of scanning electron microscopy (SEM) equipped with an EDAX Genesis EDS system. This combination of techniques allowed for a comprehensive examination of the material composition of the thin films. Operating at a scanning electron acceleration voltage of 20 kV,[37] the SEM not only provided valuable insights into the chemical composition but also allowed for a detailed assessment of the surface patterning and construction of the SnS thin films. In addition to SEM-EDX analysis, X-ray diffraction (XRD) was employed to investigate the crystal structure and preferred plane orientation of the thin films. A panalytical X-ray diffractometer, utilizing an incident Cu beam and Kα radiations (λ = 1.5406 Å), performed a 2θ scan in the range of 20–80°.[38] This meticulous structural analysis revealed crucial information about the thin films' internal structure. The Scherrer formula as presented in eqn (1)[39] was used to predict the size of the crystallite (D).[40] Where D, λ, θ, β and k represent the crystallite size, wavelength, diffraction angle, half-value width, and Scherrer constant (0.9), respectively. To calculate other structural parameters including the microstrain (ε) and dislocation density (δ) utilizing Williamson and Smallman's (WS) method, eqn (2) and (3) are used, respectively.[41]

$$D = \frac{k\lambda}{\beta \cos\theta} \quad (1)$$

$$\varepsilon = \frac{\beta \cos\theta}{4} \quad (2)$$

$$\delta = \frac{1}{D^2} \quad (3)$$

Table 1 Elemental analysis of (a) undoped and Cu-doped (b–e) SnS thin films

	Elemental composition (%)			Atomic ratio	
Sample	S	Sn	Cu	(Sn + Cu)/S	Sn/S
a	45	55	0	1.22	1.22
b	44	45	11	1.27	1.02
c	42	43	15	1.38	1.02
d	42	42	16	1.38	1.00
e	41	41	18	1.44	1.00

2.4 Optical and electrical property measurements

The measurement of optical and electrical properties is integral to understanding the suitability of Cu-doped SnS thin films for photovoltaic applications. Raman spectroscopy played a vital role in structural characterization process. Employing a Raman spectrometer with incident radiations of 530 nm wavelength at ordinary temperature, gained insights into the structural characteristics of the films. Orthorhombic SnS with 8 atoms in each unit cell following 24 ordinarily vibrating modes and the centre of the Brillouin having these modes is presented in eqn (4).[42]

$$\Gamma = 4A_g + 2B_{1g} + 4B_{2g} + 2B_{3g} + 2A_u + 4B_{1u} + 2B_{2u} + 4B_{3u} \quad (4)$$

This technique provided detailed insights into the structural characteristics and the presence of specific phases within the films. In addition to Raman spectroscopy, spectral photoconductivity measurements were conducted to assess the light sensitivity of the Cu-doped SnS thin films, performed in a controlled environment with incident light wavelengths in the range of 650–1100 nm. This technique offered valuable data on how the thin films respond to light, a critical consideration for

their application in photovoltaics.[43] To further assess their potential as light-absorbing layers, a PerkinElmer Lambda 950 UV-VIS-NIR spectrophotometer was used to measure transmission spectra in the sample compartment environment. This analysis provided insights into the optical properties of the thin films, including their ability to absorb and transmit light in the ultraviolet, visible, and near-infrared spectra.[44] The absorption factor was determined by using eqn (5) as given by Baby *et al.*[45] Where "*T*" in the relationship stands for transmission and "*t*" for thin film thickness. The absorption factor values were used to calculate the band gap energy. The optical band gap and transition were determined using the well-known Tauc's relation (eqn (6)).[46]

$$\alpha = \frac{\ln\left[\frac{1}{T}\right]}{t} \quad (5)$$

$$\alpha h\nu = B(h\nu - E_g)^n \quad (6)$$

where α, h and ν denote the absorption factor, Plank's constant, and the frequency of incident light, respectively. The constant number 'n' is dependent on the type of the transition nature (n = 1/2, 3/2) or yields a linear relationship between $(\alpha h\nu)^2$ and $h\nu$ for a smooth change from the valence to the conduction band. Furthermore, the warm probe method was employed to ascertain the conductivity type, one of the most significant physical characteristics of a semiconductor. This technique offered a means of understanding the electrical properties of the thin films, contributing to a comprehensive characterization of their optical and electrical behaviour.[47]

3. Results and discussion

3.1 Compositional analysis

In this research, the impact of varying Cu concentrations on the physical properties of SnS thin films was systematically investigated. Most physical features of materials are intricately tied to the composition and concentration of their constituent elements. Through precise control of these elemental concentrations, the ability to manipulate the material's physical characteristics is gained. To discern the effects of different Cu concentrations, an elemental analysis using Energy Dispersive X-ray (EDX) was conducted on SnS thin films doped with Cu and the elemental composition is detailed in Table 1. Notably, pristine Sn/S and Cu-doped SnS ratios in thin films placed on glass substrates exhibited a close alignment at approximately ~1. The EDX analysis has demonstrated the content of Cu in SnS thin films, which were *in situ* doped by co-evaporation of Cu metal and SnS powders at 150 °C substrate temperature. The proportion of (Sn + Cu)/S is in line with Sn/S of pristine SnS thin films. Furthermore, the variation in the profile of the metal element in SnS thin films doped with Cu is in Fig. 2. A comparison analysis of elements' concentration (%) in these thin films is given in Fig. 3. As the Cu concentration increased,

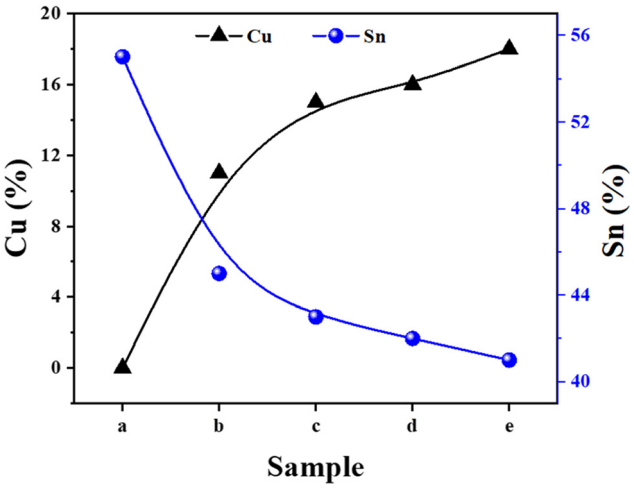

Fig. 2 Composition of metallic elements in Cu-doped SnS thin films.

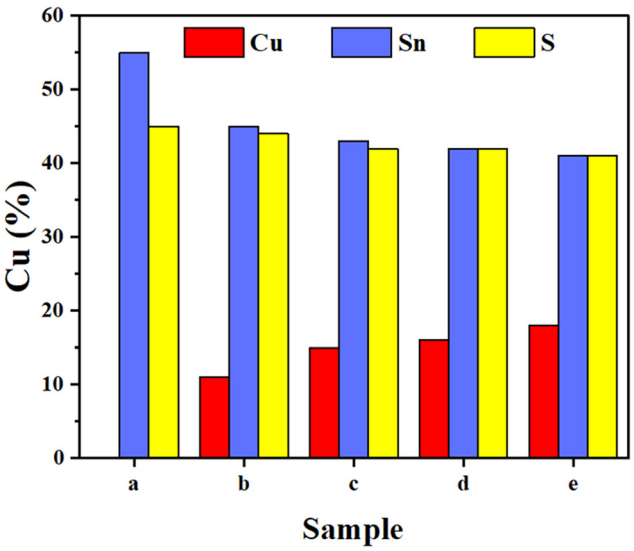

Fig. 3 Histogram presenting a comparison of elemental concentration in Cu-doped SnS thin films.

there was a noticeable reduction in the amount of Sn, suggesting that Cu atoms effectively occupied Sn lattice sites through substitutional doping. The continuous heating of the substrate at 150 °C during deposition is facilitated substitutional doping by providing sufficient energy for Cu atoms to settle within the Sn lattice sites. These results underscore the profound influence of Cu concentration on the physical features of SnS thin films, particularly in terms of their elemental composition and structure.

To provide a broader context, it's noteworthy that Baby *et al.*[45] and Reddy *et al.*[48] conducted independent studies to explore the implications of Cu-doped SnS thin films, shedding light on distinct aspects of their potential in photovoltaic applications. Baby *et al.*[45] focused on compositional analysis, investigating the impact of varying Cu concentrations in SnS thin films through EDAX mapping and point analyses. Their findings unveiled a systematic

increase in Cu concentration (atomic%) with the elevation of the DC sputtering voltage. EDAX mapping further confirmed the distribution of Cu dopant cations within the SnS film, and the atomic percentage of Cu rose from 1.4 to 10.4% as the sputtering voltage increased from 150 to 270 V. This increase in Cu content correspondingly led to a reduction in the Sn/S atomic ratio. Quantitative elemental studies were instrumental in evaluating the presence and distribution of Cu dopant cations in the films, providing clear evidence of their incorporation into the SnS matrix. In contrast, the study by Reddy *et al.*[48] delved into the influence of varying Cu concentrations on phase formation. Their comprehensive work demonstrated that higher Cu concentrations favored the formation of single-phase tetragonal-Cu_2SnS_3 thin films, while both lower and higher Cu concentrations resulted in the emergence of secondary phases. This thorough understanding of the influence of Cu concentration on phase formation and material properties contributes significantly to the potential of Cu-doped SnS thin films in the realm of photovoltaic applications.

3.2 Structural analysis

The structure of pristine SnS and Cu-doped thin films was studied with the help of the WIEN2K simulation program and the structure obtained is orthorhombic. The crystalline nature, modifications in crystalline nature, orientation of the planes, phases and effect of dopants on these structural properties were all thoroughly identified using X-ray diffraction and Raman spectroscopy.

3.2.1 X-ray diffraction. The Cu-doped SnS thin films placed on glass substrates were characterized by XRD to study the crystallographic structure and phase identification according to the concentration of the metal element Cu (%). XRD spectra obtained for these Cu-doped SnS thin films prepared with similar parameters but varying in Cu (%) are shown in Fig. 4(A). All prepared thin films are polycrystalline and the peaks in the XRD graphs in these patterns are indexed following the orthorhombic phase of pure SnS (JCPDS Card No. 39-0354). These peaks are assigned to (110), (120), (021), (111), (040), (131), (141), (002) and (110) planes of SnS having an orthorhombic crystal structure. All Cu-doped SnS thin film samples exhibit preferential orientation along the (111) plane. It is detected that the peak intensity improved and became stronger with increasing Cu concentration that is in line with the literature.[49] This behaviour is better for photovoltaic applications[50] because TFSCs based on an SnS absorbent layer[51] showed better efficiencies with films having preferential orientation along the (111) plane.[52] No elemental Cu or Sn peaks or any other phases were observed in these doped thin films, indicating the development of a pure single phase of a binary compound of SnS as a host, and effective doping of the Cu cation into SnS[53] at substitutional lattice sites.[54] The strong and sharp peak for the (111) plane of the prepared SnS doped with Cu crystalline thin films and crystallinity improved with increasing dopant concentration due to the creation of new nucleation centers.

Fig. 4(A) shows that the rising concentration of Cu doping in SnS thin films leads to an increase in peak intensity present at 31.96° corresponding to the (111) plane. This became the preferred peak with increasing Cu concentration indicating the good diffusion of elemental Cu dopant. Fig. 4(B) and (C) shows the magnified images of two peaks corresponding to the (021) and (111) planes and the observed peak shift exhibited different behaviour. The co-evaporation of Cu and SnS powders at 150 °C confirmed the doping of Cu in SnS thin films on substitutional or interstitial sites by detecting the shifting trend of these various peaks. Fig. 4(B) shows a rise in the reflection peak intensity for the (111) plane with increasing Cu concentration that clearly reveals the successful substitutional Cu atom doping on Sn lattice sites. The atomic radius of Cu (128 pm) is smaller than Sn (140 pm), then for substitutional doping, it should result in a decrease[54] in the lattice parameters of SnS. Furthermore, Fig. 4(B) shows the peak position of the (111) plane shifted towards a higher diffraction angle, which confirmed the incorporation of Cu atoms as substitutional doping at Sn sites in the SnS crystal lattice. In addition, this shift in the preferred peak's position towards a higher angle 2θ increasing the Cu concentration indicates compression in the crystal lattice with doping and reveals the successful doping of Cu at substitutional sites, which is confirmed by the literature.[55]

Furthermore, for these planes, a decrease in the interplanar spacing (d_{hkl}) was observed in the SnS crystal lattice on an increase in Cu concentration, as the ionic radii of the Cu^{++} (0.73 Å) dopant metal element are smaller than Sn^{++} (0.93 Å). In the case of substitutional doping, the lattice spacing between adjacent planes should be decreased.[56] The interplanar spacing (d_{hkl}) values corresponding to the Cu doped SnS thin films of orthorhombic crystal structures were calculated using Bragg's law $n\lambda = 2d\sin\theta$, using diffraction order $n = 1$, then "$d = \lambda/2\sin\theta$" is the interplanar spacing value, where the wavelength of X-ray radiations is equal to 1.5406 Å, and the obtained values of "d_{hkl}" are given in Fig. 5(a). This decrease in d_{hkl} is due to its inverse dependence on Bragg's angle. However, Fig. 4(C) shows that the peak position of the (021) plane shifted, with varying lower intensity, towards a lower diffraction angle end with an increase in Cu concentration, elucidating that the incorporated Cu^{2+} ions may be settled in both substitutional and interstitial sites.

However, the intensity of this peak became lower compared to an increase in Cu concentration, which shows that interstitial doping is decreased. The interstitial doping could be avoided by providing sufficient kinetic energy during deposition by increasing the substrate temperature to facilitate the substitutional Cu doping at Sn sites[55] due to the variation in their ionic radii.[57] In this work, we deposited all thin films at 150 °C substrate temperature to minimize the doping at interstitial sites. The crystallite size, micro strains, dislocation density and *d*-spacing obtained are shown in Table 2. Crystallite size first increased with Cu doping, but then decreased from 30.5 to 22 nm with increasing Cu concentration in SnS thin films. This reduction in crystallite size is due to the integration of Cu^{++} ions into the Sn^{++} sites in the SnS crystal lattice. Variation in crystallite size is shown in Fig. 5(b). A similar

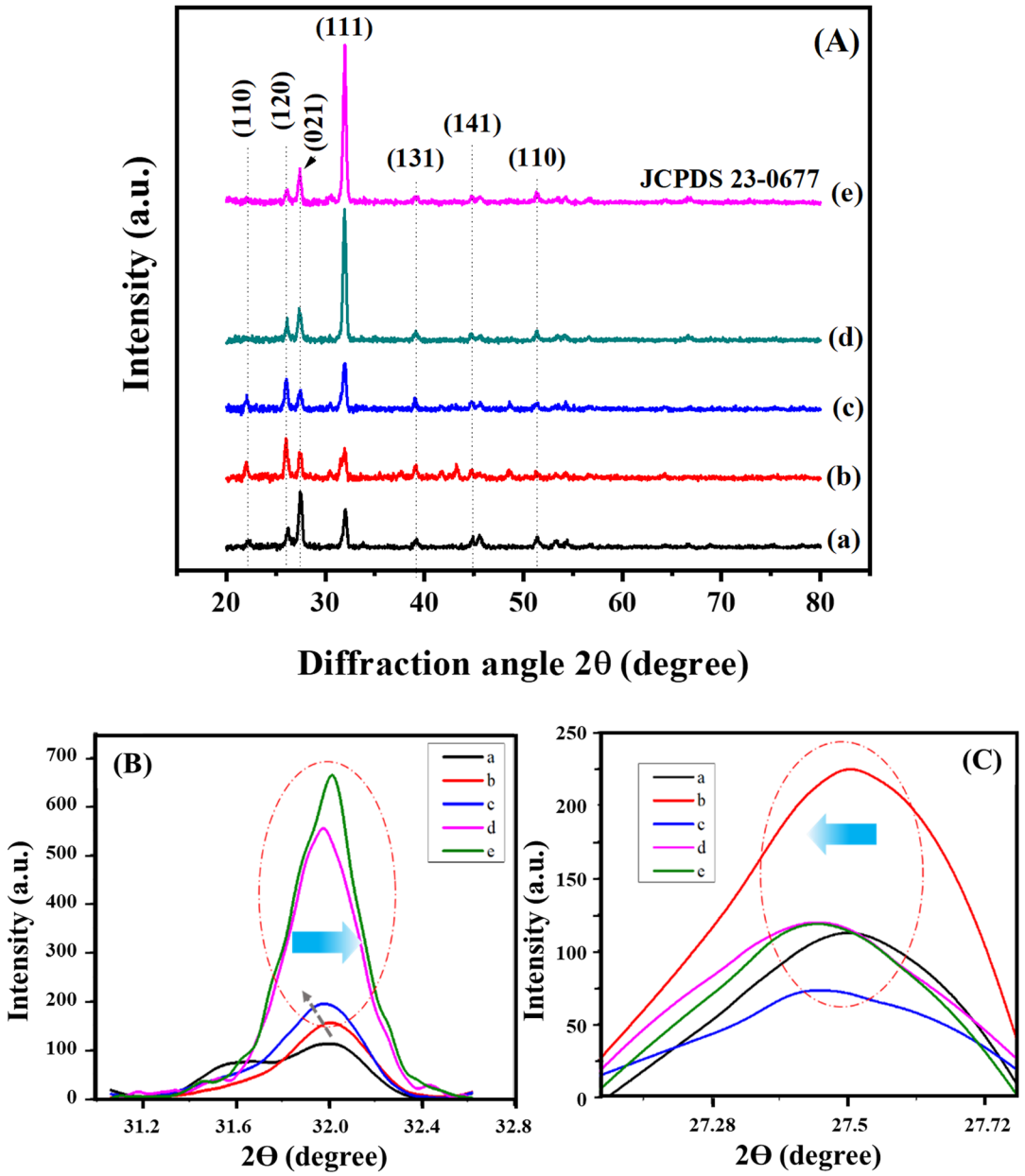

Fig. 4 (A) XRD spectra of pristine and Cu-doped SnS thin films having different Cu concentrations, (B) magnified peaks for the (111) plane and (C) magnified peaks for (021) planes.

trend was observed by other researchers for metal ion doping in sulfide binary compounds.[55] Initially, a decrease in these microstructural parameters was observed but then an increase was noticed with increasing Cu concentration that decreased lattice imperfections like defects and gaps. These microstructural parameters of the thin films characterized are shown in Table 2. The results obtained confirmed results already reported for metal ion doping in sulfide binary compounds.[58]

3.2.2 Raman spectroscopy. Raman spectroscopy is a suitable technique for diagnosing the crystal structure and investigating the phases present in synthesized materials. It facilitates the analysis of phonon band vibrations and the positions of spectral peaks. Raman spectral peaks exhibit high sensitivity to the arrangement, length, and strength of these chemical bonds in the sample material, and they are dependent on the chemical composition. Consequently, this efficient and highly sensitive characterization technique allows for the identification of the growth of any impurity phase. In the study, Raman scattering measurements were conducted on undoped and doped SnS thin films with varying Cu concentrations at ordinary temperatures. Fig. 7 illustrates the Raman spectrum of these SnS thin films, which were obtained in the 10–700 cm^{-1} wavelength range.

In these spectra, a prominent SnS characteristic peak located at approximately 160 cm^{-1} was observed, corresponding to the

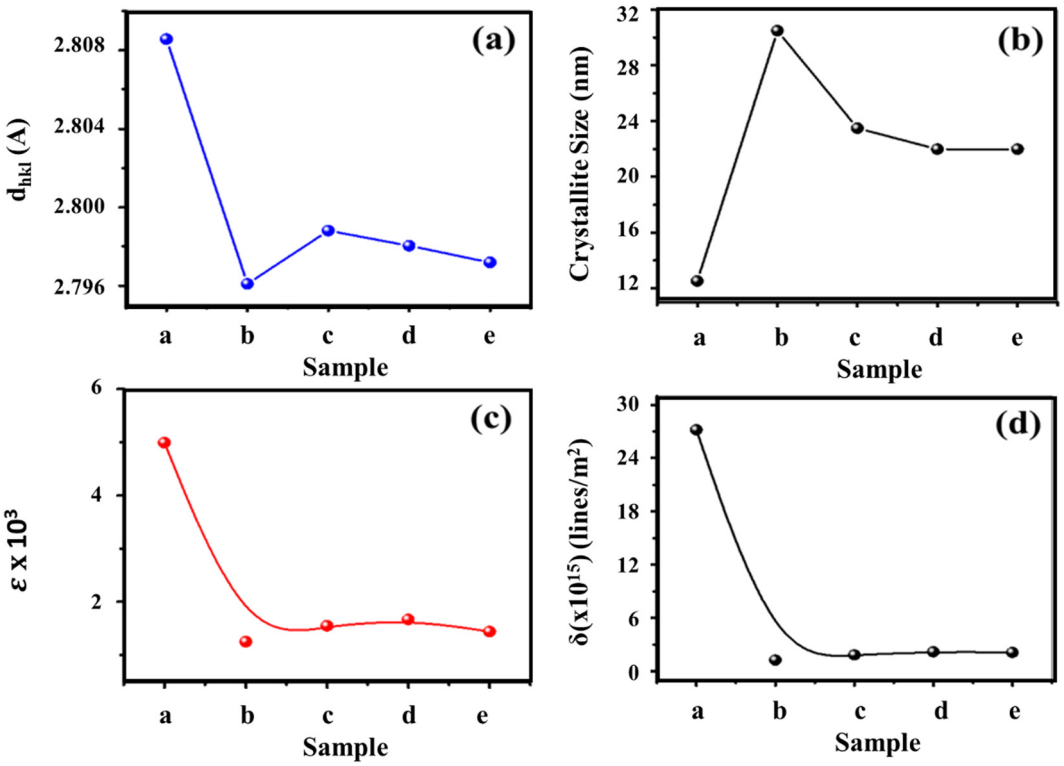

Fig. 5 Structural parameters of pristine and Cu-doped SnS thin films; (a) interplanar spacing (d_{hkl}), (b) crystallite size (D), (c) microstrain (ε) and (d) dislocation density (δ).

Table 2 Microstructural parameters of (a) undoped and (b–e) Cu-doped SnS thin films

	Microstructural parameters			
Sample	Interplanar spacing d_{hkl} (Å)	Crystallite size D (nm)	Microstrain (ε) $\times 10^{-3}$	Dislocation density (δ) $\times$ 10^{15} (lines m^{-2})
a	2.80856	12.5	4.99	27.185
b	2.79609	30.5	1.25	1.240
c	2.79880	23.5	1.55	1.825
d	2.79804	22.1	1.67	2.160
e	2.79719	22.0	1.44	2.100

distinct vibrational Raman dynamic mode B_{3g} of orthorhombic SnS.[59] The peak position varied with Cu concentration in Cu-doped SnS thin films, which confirms the settlement of Cu atoms at Sn sites in the SnS lattice crystal. Notably, not phase-related peaks were observed, further confirming the absence of Cu-related phases such as SnS_2 and Sn_2S_3. These results confirmed the preparation of pure SnS thin films doped with Cu metal. As shown in Fig. 6, upon initial Cu doping, the peak intensity decreased and gradually improved with increasing Cu concentration. This modification in peak intensity supported the presence of Cu in these films. Furthermore, Fig. 6 shows a red shift in the peaks for increased Cu concentration. This shift may be attributed to phonon localization within nanostructure boundaries, possibly induced by defects and spatial confinement.

From these results, it can be deduced that the relationship between the intensity of the SnS characteristic peak and Cu concentration can be attributed to physical mechanisms associated with the incorporation of copper into the SnS thin films. Initially, the introduction of Cu disrupts the crystal lattice, introducing disorder and defects, resulting in a lower intensity of the SnS characteristic peak. This disruption influences the phonon vibrations and, consequently, the Raman spectrum, causing a reduction in peak intensity. However, as the Cu concentration increases, more Cu atoms become integrated into the SnS lattice, leading to an improved crystal quality and structural order. This gradual recovery of the crystal structure enhances phonon vibrations and, subsequently, increases the peak intensity. The observed red shift in the peak position with increasing Cu concentration suggests changes in the material's crystal structure or phonon dynamics.[60] In summary, the presence of Cu initially disrupts the crystal lattice, causing a decrease in peak intensity. However, the gradual improvement is a result of enhanced crystal quality and phonon vibrations as Cu concentration increases, making the SnS characteristic peak a valuable indicator of Cu concentration and its impact on the material's properties.

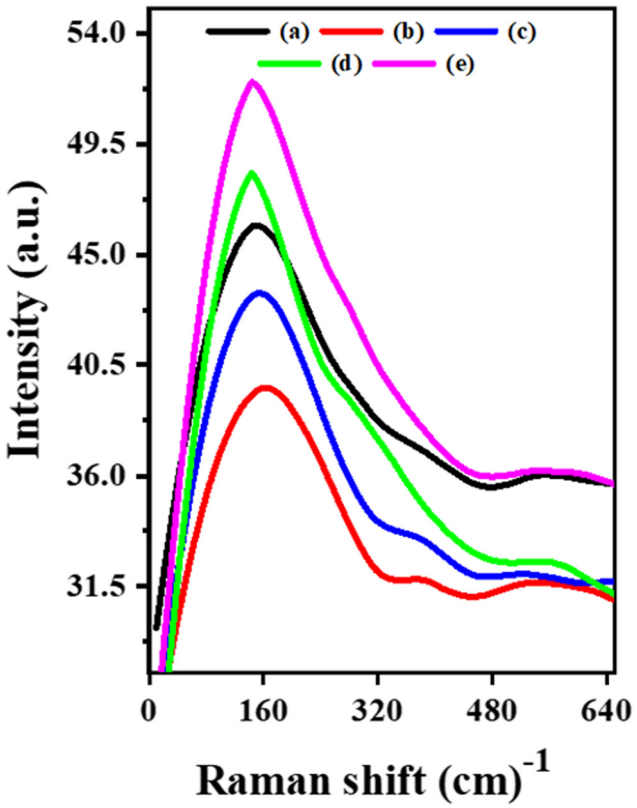

Fig. 6 Raman spectra of (a) undoped and (b)–(e) Cu-doped SnS thin films.

3.3 Surface morphology

Scanning electron microscopy (SEM) is a fantastic tool for researching the surface morphology of thin films. SEM provides essential information about the shape of particles, their size and distribution. Surface morphology has a prominent impact on physical properties that influence photovoltaic and other optoelectronic applications of these thin films. As-prepared and Cu-doped SnS thin films were characterized using SEM with low magnification and are shown in Fig. 7(a)–(e). The energy of the incident electron beam, magnification and scale were 20.0 kV, ×1000 and 20 μm, respectively, and are shown in Fig. 7(a)–(e). These SEM images made it abundantly clear that the Cu-doped SnS thin films are well compacted and have a consistent surface morphology in their as-deposited state. It can also be seen that these thin films are made up of uniform particles. However, compact morphology and homogeneous settlement of particles after the Cu doping remained intact.

This evocative revelation draws parallels to the pioneering work of Mathews and colleagues,[61] who ventured into the world of TiO_2 thin films through the sol–gel dip coating technique. Their findings showcased uniformity and strong adhesion, where film thickness grew with the number of deposition cycles, eventually reaching an average of 650 nm after four cycles. Interestingly, annealing at 400 °C led to a reduction in thickness. In a different vein, researchers have laid bare the effects of Cu doping on the grain size and overall morphology of SnS thin films. Jain *et al.*'s study[62] unveiled the complex

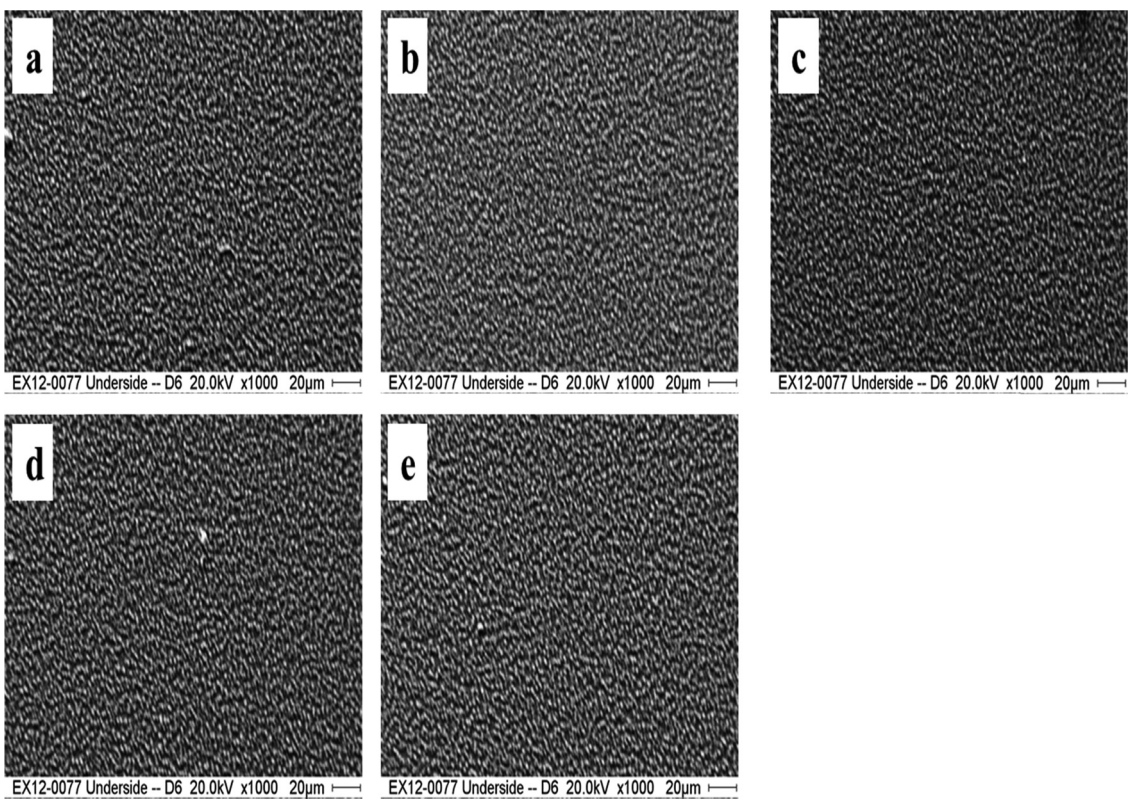

Fig. 7 SEM images of (a) undoped and (b)–(e) Cu-doped SnS thin films.

relationship between grain size, film thickness, annealing temperature, and band-gap alterations. These alterations are indicative of Cu doping's influence on crystal potential and, consequently, grain size. Bommireddy *et al.*[63] further underscored the profound effects of Cu doping on the crystalline state of SnS thin films. Here, it was observed that increasing the Cu doping concentration initially augmented the grain size, followed by a subsequent reduction with further doping increases. This variation in grain size can be attributed to lattice dilatation, engendered by Cu doping. The significance of discussing these surface changes by referencing pertinent literature cannot be overstated.

Notably, our exploration into the impact of Cu doping on thin film morphology aligns with Mathews *et al.*'s work,[61] where Cu doping similarly left the morphology of TiO_2 thin films largely untouched. The journey to creating these Cu-doped SnS thin films involved the simultaneous resistive heating of Cu and SnS powders to 150 °C, with varying Cu content, and their application to glass substrates. The SEM images, a testament to our methodology, showcased remarkable compactness and seamless distribution of crystallites. Furthermore, these images were devoid of any agglomerations, islands, voids, or cavities, affirming the formation of uniform thin films. This endeavour in *in situ* substitutional Cu doping at SnS crystal lattice sites was underpinned by the precise manipulation of substrate temperature, ensuring that dopant atoms found their designated sites while preventing interstitial doping or the emergence of unwanted additional phases.[22]

3.4 Optical analysis

For investigation of optical parameters like % transmission, absorption coefficient, and SnS thin films with undoped and Cu-doped optical bandgap, transmission spectra of these samples were used. All thin films' optical measurements were performed at room temperature. The UV-VIS-NIR transmission measurements were made in the 280–3300 nm range. Fig. 8 shows the variation in transmission spectra against the incident wavelength (nm) of the Cu-doped SnS films. These spectra revealed that the transmission, absorption edge and quality of the thin films depend on Cu concentration. The excellent quality and homogeneity of these thin films are manifested by the appearance of interference fringes and the presence of maxima and minima in the transmission spectra with increasing Cu concentration confirming dependency on Cu concentration. Fig. 8 clearly shows that these films have a low transmission for the incident light in the wavelength scope of 280 to 1250 nm. This behaviour indicates that these films are good for absorption of the sunlight in this region of the solar spectrum.

Furthermore, the absorption edge moved to a lower wavelength, demonstrating the ability of the deposited thin films to absorb the high-energy portion of the solar spectrum. For the optical band gap, the curves of $(\alpha h\nu)^2$ and light energy $h\nu$ were plotted in this work and reproduced as seen in Fig. 9. A linear behaviour was shown for the low energy photons of incident light by all the curves. As shown, the Tauc's relation holds good

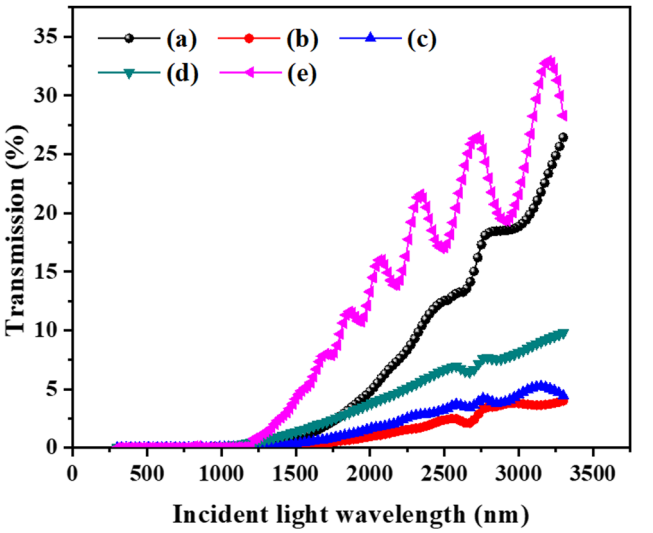

Fig. 8 Transmission spectra of (a) undoped and (b)–(e) Cu-doped SnS thin films.

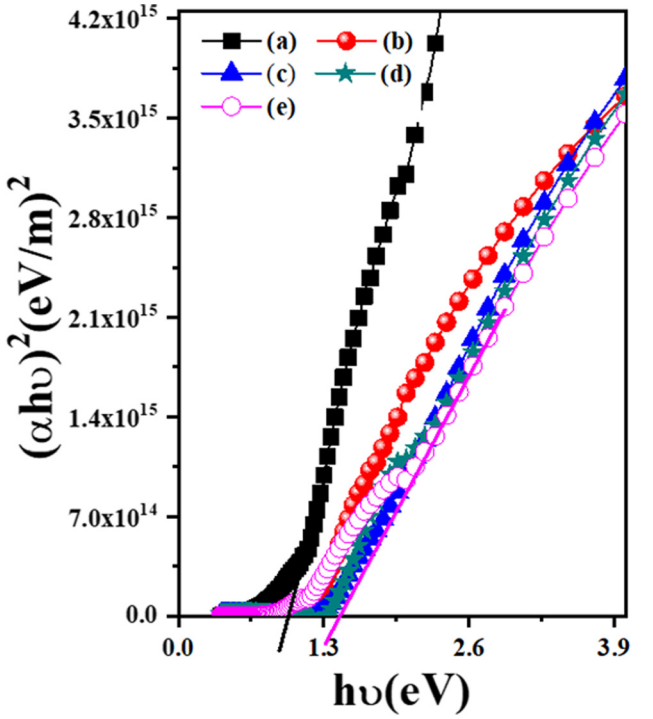

Fig. 9 Bandgap determination for SnS thin films doped with Cu concentrations.

for these SnS and Cu-doped SnS thin films when '$n = \frac{1}{2}$'. The results support that these thin films' optical transition is, therefore, direct transition. By extending the linear portion of the absorption curve, the direct band gap energy value has been determined by its intercept to the energy axis (x-axis), *i.e.*, (in eqn (6) $h\nu = E_g$ for absorption factor $\alpha = 0$), as shown in Fig. 9. The calculated values of E_g are given in Table 3.

Table 3 Values of energy for band gaps for different concentrations of Cu doping in SnS

Sample	Cu (%)	(eV)
a	0	1.10
b	11	1.18
c	15	1.33
d	16	1.39
e	18	1.47

These obtained results showed that the value of E_g is dependent on Cu concentration. Doped semiconducting materials having a direct bandgap are active and useful for optoelectronic devices.[64] Thus, doped-SnS is a better candidate for solar cell uses of light absorption. The results reported in this work are in agreement with previously reported literature for doped[65] and undoped SnS.[66]

Fig. 10 shows the variation of E_g with an atomic percentage of Cu concentration in the Cu-doped SnS thin films. Fig. 10 and data given in Table 3 showed that the E_g value is higher for higher Cu concentrations. SnS thin films' optical bandgap energy increased with increasing Cu content. As a result, a blue optical bandgap energy shift has been observed in SnS thin films and is attributed to Cu doping. That there are no deep defect states created during doping was confirmed by the observed shift in the optical bandgap on Cu doping. The same pattern was reported by Patel *et al.*[57] for SnS thin films prepared by the compressed air-assisted chemical spray pyrolysis (CSP) and *ex situ* SnS thin films doped with Cu by pulsed Direct-Current magnetron sputtering, where E_g increased from 1.44 to 1.66 eV. Furthermore, a similar blue shift response was observed in Pb-doped SnS thin films, where E_g has risen from 1.22 to 1.32 eV on doping. In addition, similar observations were reported previously,[45] where the E_g increased from 1.34 to 1.43 eV after Ag doping in SnS thin films. The same trends[67] have been observed for Cu-doped SnS thin films by other researchers.[68] A reduction in E_g and red shift was also observed by Sebastian *et al.*[69] for Al doping in SnS thin films, where the value of E_g reduced from 1.5 to 1.29 eV. The reason could be the smaller ionic radius of Al^{3+} (53 pm) in comparison to the ionic radii of Cu^{+} (77 pm), Ag^{+} (115 pm) and Pb^{2+} (119 pm) along with shallow levels in the band gap region.

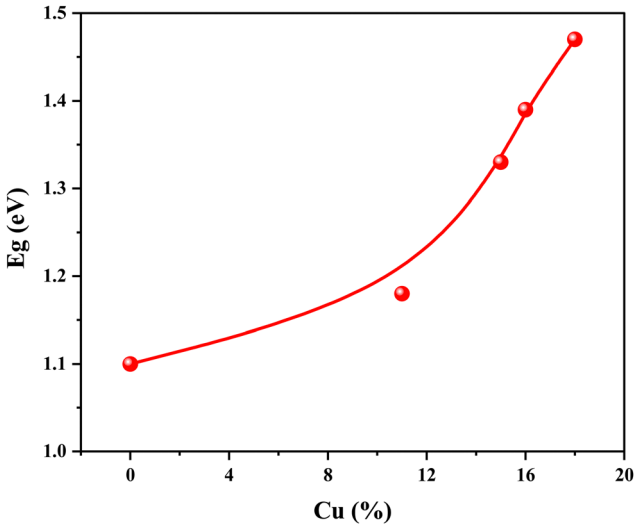

Fig. 10 Dependence of bandgap energy on doped Cu concentration in SnS thin films.

3.5 Conductivity-type determination

The conductivity type is a fundamental property of semiconductor materials that plays a crucial role in various applications. Different techniques are employed to determine the conductivity type. The intercalation technique, for instance, introduces Cu atoms into SnS thin films, causing the s-orbital electrons of Cu atoms to extend into conduction bands of SnS. This effectively reduces the bandgap and induces p-type semiconductor behaviour. In addition to intercalation, several chemical doping techniques have been developed to enhance the electrical and optical properties of SnS thin films. These methods involve processes such as absorbing NO_2 molecules, depositing potassium (K), applying organic molecular films, immersing in organic solutions, and treating the surface with organic superacids, all of which effectively dope the films and enhance their electrical and optical performance. Furthermore, alloying SnS with copper (Cu) using various synthesis methods like mechanical exfoliation, physical vapour deposition (PVD), and chemical vapour deposition (CVD) can modify the charge-conductive states of SnS thin films, resulting in p-type semiconductor behaviour.[70] For this study, the hot probe method was used to identify the conductivity type. One of the advantages of the hot probe method compared to other techniques is its non-destructive nature. Unlike some methods that may require altering the material or involving chemical processes, the hot probe method can provide valuable information about the conductivity type without introducing any significant changes to the sample.[71] This makes it a practical and minimally invasive choice for conductivity-type determination in semiconductor materials. All the Cu-doped SnS thin films showed the conductivity type to be p-type. The hot probe set-up used during characterization is shown in Fig. 11. To determine the conductivity type and to examine the photo response, circular contacts of Molybdenum (Mo) were deposited on the top of the film surfaces at the chamber ambient temperatures by DC magnetron sputtering. Every contact deposited has an area of 3.14 mm^2 and was separated by a distance of 3 mm. Researchers prepared SnS thin films doped with Cu by different methods and provided different treatments after doping, as presented in Table 4. This comparison demonstrated how the deposition and doping processes affect the physical properties of these thin films.

3.6 Spectral photoconductivity

Spectral photoconductivity measurements were used to examine the application of the prepared Cu-doped SnS thin films as light-absorbing layers, providing valuable insights into newly synthesized semiconductor materials.[72] This technique allows

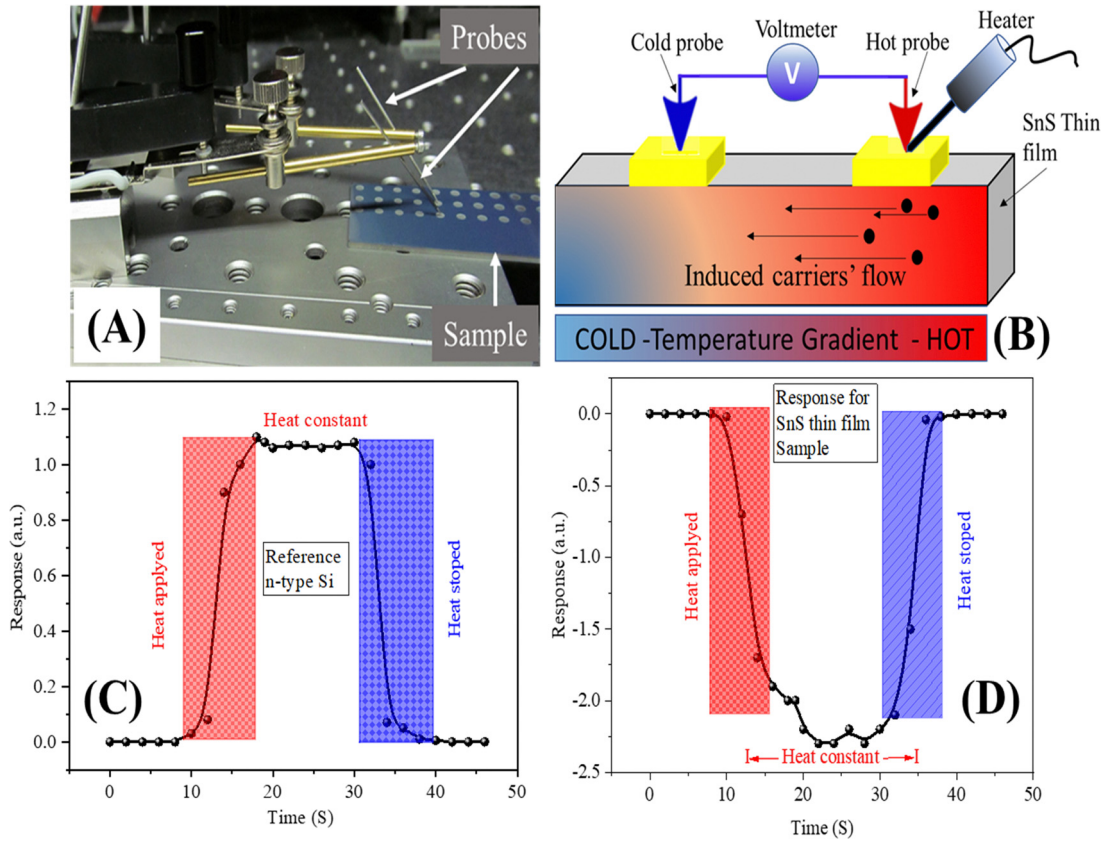

Fig. 11 Conductivity type determination; (A) measurement set-up, (B) induced charge carriers and their flow, (C) response for n-type Si and (D) response for p-type Cu-doped SnS studied.

Table 4 Cu doping in SnS thin films by different methods

SnS thin film deposition method	Cu doping method	Cu doping (%)	Crystallite size (nm)	Band gap energy (eV)	Conductivity type	Ref.
Chemical spray pyrolysis method (CSP), (Sn : S) = 0.1 : 0.1, 0.1 : 0.2, 0.1 : 0.3 and 0.1 : 0.4.	$CuCl_2 \cdot 2H_2O$ used in precursor solution	Cu fixed 4% of Sn concentration	—	1.3–1.7	n-type	61
Electrodeposition	$CuCl_2$ content of 0.00625, 0.0125, 0.025, and 0.05 mM			1.31–0.97		62
Spray pyrolysis	0.05 M $CuCl_2 \cdot 2H_2O$ aqueous solution was added to spray solution	4%, 8%	22.9–19.8	1.83–1.90	p-type	63
Ultrasonic spray pyrolysis (USP) technique	$(SnCl_2–2H_2O)$ precursor was dissolved in deionized water	[Cu]/[Sn] = 2%, 5% and 10%	—	1.82–2.2	—	64
Thermal evaporation technique	Cu films were deposited on the SnS films	5.7, 15, 23 atom %	45.95, 68.91, 78.74	1.49, 1.38, 1.71	p-type	65
DC-RF magnetron co-sputtering technique	DC-RF magnetron co-sputtering technique	4.8%	26	1.33	p-type	51
Thermal evaporation	Co-evaporation, *in situ* doping	18%	22	1.47	p-type	Present work

for precise assessment of photoconductive behaviour within the spectral range of 650 to 1100 nanometers (nm). The maximum photoconductive response, corresponding to the band gap of the thin films, was consistently observed at around 900 nm, showcasing sensitivity to both incident light energy and the band gap of the material. The band gap energy was established as Cu concentration-dependent. Increasing the concentration of Cu in the SnS material led to a noticeable reduction in the band gap energy. This reduction is attributed to the introduction of Cu atoms, which effectively alters the material's electronic structure, requiring less energy for charge carriers to transition from the valence band to the conduction band (Fig. 12).

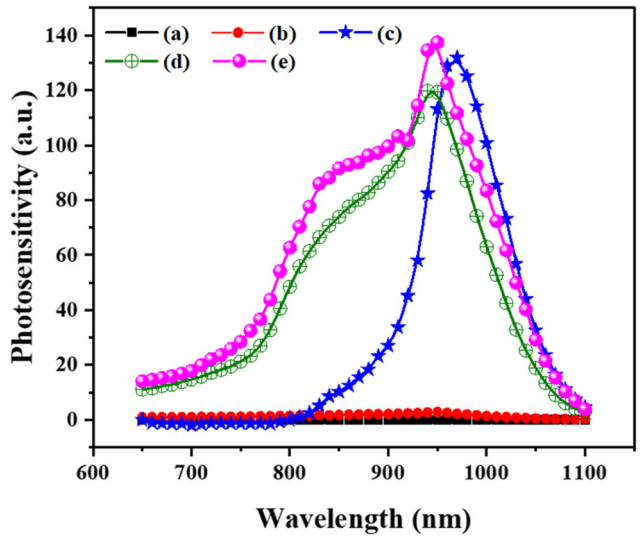

Fig. 12 Photo response of (a) undoped and (b)–(e) Cu-doped SnS thin films.

This relationship between band gap energy and the observed photoconductive response is closely intertwined. The photoconductive response represents the material's capacity to generate and transport charge carriers when exposed to light. In Cu-doped SnS thin films, a decreased band gap energy, resulting from higher Cu concentrations, fosters more efficient charge carrier generation upon light absorption, evident in the enhanced photoconductive response. Addressing the low photosensitivity observed in dopant-free SnS thin films and those with lower Cu concentrations, this phenomenon can be linked to the scarcity of generated charge carriers. Dopant-free SnS thin films, with limited Cu content, exhibit a lower number of free charge carriers due to their wider band gap, necessitating higher energy input for electron transitions upon exposure to light.

Conversely, increased Cu content in SnS thin films narrows the band gap, leading to a higher concentration of charge carriers excitable by incident light, ultimately enhancing photosensitivity. The correlation between band gap energy, Cu concentration, and the number of generated charge carriers is pivotal in understanding the observed photoconductive behaviour in Cu-doped SnS thin films.[73] Additionally, it's important to note that band gap energy is influenced not only by Cu concentration but also by grain size and grain boundaries (Fig. 12). Smaller grain sizes and well-defined grain boundaries contribute to alterations in the material's electronic properties, impacting the band gap. This intricate relationship among band gap energy, Cu concentration, grain size, and grain boundaries is crucial in comprehending the observed photoconductive behaviour in Cu-doped SnS thin films.

4. Conclusion

Cu-doped SnS thin films were successfully deposited on glass substrates at a controlled temperature of 150 °C by co-evaporating Cu and SnS powders, with varying Cu content. The resulting films exhibited a polycrystalline structure with a preferential orientation along the (111) plane. Quantitative X-ray diffraction analysis revealed an increase in peak intensity with higher Cu concentrations, particularly relevant for photovoltaic applications. Thin-film solar cells with (111) plane orientation in the SnS absorptive layer have shown improved efficiency. Raman spectroscopy confirmed the purity of the samples, with no other phases detected besides SnS. Scanning electron microscopy revealed compact and uniform surface morphology in both undoped and Cu-doped SnS films. The *in situ* Cu-doping process did not disrupt the films' homogeneity. The photoconductivity response correlated directly with Cu content, with optimal response occurring at 900 nm, aligning with the most intense part of the solar spectrum. The direct bandgap of SnS films depended on Cu content, ranging from 1.10–1.47 eV for Cu concentrations from 0 to 18 at%. These quantitative results highlight the significant influence of Cu doping on the films' optical properties. All samples consistently displayed p-type conductivity, both before and after doping, confirmed by the hot probe method. These comprehensive studies on Cu-doped SnS thin films provide strong evidence of enhanced physical properties through Cu doping. This enhancement positions them as a promising choice for an active photon-absorbing layer in solar cell materials. In the broader context of solar cell materials, these findings hold profound implications, offering a pathway to improve the efficiency and viability of thin-film solar cell technologies. This advancement contributes to the progress of sustainable and renewable energy sources.

Author contributions

Ghulam Hasnain Tariq, Ghulam Asghar, M. Shahzad Shifa: (Conceptualization, investigation, formal analysis, methodology, writing – original draft). Visualization: lead; writing – original draft: lead), M. Anis-Ur-Rehma, Sana Ullah, Zulfiqar Ali Shah: (Investigation, software Resources, supervision validation, writing – original draft). Imane Ziani, Ahmed M. Tawfeek: (Conceptualization, investigations, visualization, resources, supporting, writing, funding formal analysis, software). Farooq Sher (Conceptualization, funding acquisition, investigation, project administration, resources, supervision, writing – original draft, writing – review & editing).

Conflicts of interest

The authors declare that they have no known competing financial interests or personal relationships that could have appeared to influence the work reported in this paper.

Acknowledgements

The authors are thankful to the Researchers Supporting Project No. (RSPD2023R672), King Saud University, Riyadh, Saudi

Arabia for the financial support. Ghulam Hasnain Tariq acknowledges the Higher Education Commission (HEC) of Pakistan for the funding received through NRPU Project No: 10304/Punjab/NRPU/R&D/HEC/2017. Sana Ullah acknowledges HEC Pakistan for funding received through NRPU Project No: 20-14709/NRPU/R&D/HEC/2021. Both authors thankfully appreciate and acknowledge HEC for promoting the research environment through project funding schemes. The authors are thankful to Dr David Lane, Cranfield University, UK and Dr Nazir Abbas, COMSATS University Islamabad for providing characterization facilities.

References

1 A. Tawfik, X. Tan, M. Elsamadony, M. A. Qyyum, A. M. Azzam, M. Mubashir, H. S. Ng, M. S. Akhtar and K. S. Khoo, Graphene/hydroxyapatite nano-composite for enhancement of hydrogen productivity from delignified duckweed, *Fuel*, 2022, **330**, 125537.

2 C. Te Hsieh, P. Y. Sung, Y. A. Gandomi, K. S. Khoo and J. K. Chang, Microwave synthesis of boron- and nitrogen-codoped graphene quantum dots and their detection to pesticides and metal ions, *Chemosphere*, 2023, **318**, 137926.

3 Y. G. Song, I.-H. Baek, J.-G. Yim, T. Eom, T.-M. Chung, C.-H. Lee, C. S. Hwang, C.-Y. Kang and S. K. Kim, Cross-linked structure of self-aligned p-type SnS nanoplates for highly sensitive NO 2 detection at room temperature, *J. Mater. Chem. A*, 2022, **10**, 4711–4719.

4 J.-H. Ahn, M.-J. Lee, H. Heo, J. H. Sung, K. Kim, H. Hwang and M.-H. Jo, Deterministic two-dimensional polymorphism growth of hexagonal n-type SnS2 and orthorhombic p-type SnS crystals, *Nano Lett.*, 2015, **15**, 3703–3708.

5 S. Sohila, M. Rajalakshmi, C. Ghosh, A. K. Arora and C. Muthamizhchelvan, Optical and Raman scattering studies on SnS nanoparticles, *J. Alloys Compd.*, 2011, **509**, 5843–5847.

6 Z. Xiao, F.-Y. Ran, M. Liao, H. Hiramatsu, K. Ide, H. Hosono and T. Kamiya, Multiple states and roles of hydrogen in p-type SnS semiconductors, *Phys. Chem. Chem. Phys.*, 2018, **20**, 20952–20956.

7 W. Yang, L. Gan, H. Li and T. Zhai, Two-dimensional layered nanomaterials for gas-sensing applications, *Inorg. Chem. Front.*, 2016, **3**, 433–451.

8 F. Teng, K. Hu, W. Ouyang and X. Fang, Photoelectric detectors based on inorganic p-type semiconductor materials, *Adv. Mater.*, 2018, **30**, 1706262.

9 H. Kafashan, Optoelectronic properties of In-doped SnS thin films, *Ceram. Int.*, 2019, **45**, 334–345.

10 S. L. Mousavi, F. Jamali-Sheini, M. Sabaeian and R. Yousefi, Enhanced solar cell performance of P3HT: PCBM by SnS nanoparticles, *Sol. Energy*, 2020, **199**, 872–884.

11 Ş. Baturay, A. Tombak, D. Batibay and Y. S. Ocak, n-Type conductivity of CuO thin films by metal doping, *Appl. Surf. Sci.*, 2019, **477**, 91–95.

12 N. K. Singh, S. Bathula, B. Gahtori, K. Tyagi, D. Haranath and A. Dhar, The effect of doping on thermoelectric performance of p-type SnSe: Promising thermoelectric material, *J. Alloys Compd.*, 2016, **668**, 152–158.

13 X. Liu, C. Chen, L. Wang, J. Zhong, M. Luo, J. Chen, D. Xue, D. Li, Y. Zhou and J. Tang, Improving the performance of Sb_2Se_3 thin film solar cells over 4% by controlled addition of oxygen during film deposition, *Prog. Photovoltaics*, 2015, **23**, 1828–1836.

14 H. Tian, X. Meng, J. Yang, C. Fan, S. Yuan, X. An, C. Sun, Y. Zhang, M. Wang and H. Zheng, Visible phototransistors based on vertical nanolayered heterostructures of SnS/SnS2 p–n and SnSe2/SnS2 n–n nanoflakes, *ACS Appl. Nano Mater.*, 2020, **3**, 6847–6854.

15 K. T. R. Reddy, N. K. Reddy and R. W. Miles, Photovoltaic properties of SnS based solar cells, *Sol. Energy Mater. Sol. Cells*, 2006, **90**, 3041–3046.

16 S. Sebastian, S. Vinoth, K. H. Prasad, M. S. Revathy, S. Gobalakrishnan, P. K. Praseetha, V. Ganesh and S. AlFaify, Quantitative analysis of Ag-doped SnS thin films for solar cell applications, *Appl. Phys. A: Mater. Sci. Process.*, 2020, **126**, 1–12.

17 F.-H. Wang, M.-S. Chen, Y.-L. Jiang, H.-W. Liu and T.-K. Kang, Fabrication and characterization of sputtered Mg and F co-doped ZnO thin films with different substrate temperature for silicon thin-film solar cell applications, *J. Alloys Compd.*, 2022, **897**, 163174.

18 M. Shkir, I. M. Ashraf, K. V. Chandekar, I. S. Yahia, A. Khan, H. Algarni and S. AlFaify, A significant enhancement in visible-light photodetection properties of chemical spray pyrolysis fabricated CdS thin films by novel Eu doping concentrations, *Sens. Actuators, A*, 2020, **301**, 111749.

19 C. M. Muiva, T. S. Sathiaraj and K. Maabong, Effect of doping concentration on the properties of aluminium doped zinc oxide thin films prepared by spray pyrolysis for transparent electrode applications, *Ceram. Int.*, 2011, **37**, 555–560.

20 A. Loukil, A. Boukhachem, M. Ben Amor, M. Ghamnia and K. Raouadi, Effects of potassium incorporation on the structural, optical, vibrational and electrical properties of NiO sprayed thin films for p-type optical windows, *Ceram. Int.*, 2016, **42**, 8274–8289.

21 S. Sujatha Lekshmy and K. Joy, Structural and optoelectronic properties of indium doped SnO 2 thin films deposited by sol gel technique, *J. Mater. Sci.: Mater. Electron.*, 2014, **25**, 1664–1672.

22 N. Spalatu, J. Hiie, R. Kaupmees, O. Volobujeva, J. Krustok, I. Oja Acik and M. Krunks, Postdeposition processing of SnS thin films and solar cells: prospective strategy to obtain large, sintered, and doped SnS grains by recrystallization in the presence of a metal halide flux, *ACS Appl. Mater. Interfaces*, 2019, **11**, 17539–17554.

23 G. G. Ninan, C. S. Kartha and K. P. Vijayakumar, On the preparation of n-type SnS: Cu using chemical spray pyrolysis for photovoltaic application: Effect of annealing, *Sol. Energy Mater. Sol. Cells*, 2016, **157**, 229–233.

24 A. Alasvand and H. Kafashan, Investigation the effect of Pb incorporation on the surface characterizations of

electrodeposited CdSe nanostructures, *J. Alloys Compd.*, 2020, **817**, 152711.

25 A. A. Aboud, A. Mukherjee, N. Revaprasadu and A. N. Mohamed, The effect of Cu-doping on CdS thin films deposited by the spray pyrolysis technique, *J. Mater. Res. Technol.*, 2019, **8**, 2021–2030.

26 F. J. Willars-Rodríguez, I. R. Chávez-Urbiola, M. L. Melgoza-Ramírez, L. E. Trujillo, E. A. Chávez-Urbiola, R. Ramírez-Bon, P. Vorobiev and Y. V. Vorobiev, Research implementing different dopants (M = Al, Sn, and Eu) on the properties of Schottky diodes with structure TCO/CdS/C and TCO/CdS: M/C, *J. Alloys Compd.*, 2022, **894**, 162369.

27 K. Usharani and A. R. Balu, Structural, optical, and electrical properties of Zn-doped CdO thin films fabricated by a simplified spray pyrolysis technique, *Acta Metall. Sin. (Engl. Lett.)*, 2015, **28**, 64–71.

28 K. C. Dubey, A. Zaidi and R. R. Awasthi, Environmentally benign structural, topographic, and sensing properties of pure and Al-doped ZnO thin films, *ACS Omega*, 2022, **7**, 28946–28954.

29 A. Javed and M. Bashir, Controlled growth, structure and optical properties of Fe-doped cubic π-SnS thin films, *J. Alloys Compd.*, 2018, **759**, 14–21.

30 A. K. Sen Gupta, S. F. U. Farhad, M. S. Habib, M. R. Hossan, K. Hossain, N. K. Das, M. Quamruzzaman, M. A. Matin and N. Amin, Characterizations of extrinsically doped CZTS thin films for solar cell absorbers fabricated by sol-gel spin coating method, *Appl. Surf. Sci. Adv.*, 2023, **13**, 100352.

31 F. Aslan, F. Arslan, A. Tumbul and A. Goktas, Synthesis and characterization of solution processed p-SnS and n-SnS2 thin films: Effect of starting chemicals, *Opt. Mater.*, 2022, **127**, 112270.

32 M. Ohring, *Materials Science of Thin Films: Depositon and Structure*, Elsevier, 2001.

33 G. H. Tariq, K. Hutchings, D. W. Lane, K. D. Rogers and M. Anis-ur-Rehman, Annealing effects on the microstructural properties of complex sulfosalt (SnS) x–(Bi_2S_3) $1-x$ gradient thin films, *J. Phys. D: Appl. Phys.*, 2013, **46**, 485302.

34 J. Kennedy, P. P. Murmu, J. Leveneur, A. Markwitz and J. Futter, Controlling preferred orientation and electrical conductivity of zinc oxide thin films by post growth annealing treatment, *Appl. Surf. Sci.*, 2016, **367**, 52–58.

35 S. S. Hegde, A. G. Kunjomana, P. Murahari, B. K. Prasad and K. Ramesh, Vacuum annealed tin sulfide (SnS) thin films for solar cell applications, *Surf. Interfaces*, 2018, **10**, 78–84.

36 S. L. Mousavi, F. Jamali-Sheini, M. Sabaeian and R. Yousefi, Correlation of Physical Features and the Photovoltaic Performance of P3HT: PCBM Solar Cells by Cu-Doped SnS Nanoparticles, *J. Phys. Chem. C*, 2021, **125**, 15841–15852.

37 G. G. Ninan, C. SudhaKartha and K. P. Vijayakumar, Synthesis Of Spray Pyrolysed Copper Doped Tin Sulfide (SnS: Cu) Thin Films By Optimizing The Anionic Precursor Molarity, *Mater. Today Proc.*, 2019, **8**, 352–356.

38 Y. Liu, K. Cao, J. Liu, Z. Zhang, J. Ji, F. Wang and Z. Li, Electrodeposition of copper-doped SnS thin films and their electric transmission properties control for thermoelectric enhancement, *J. Mater. Sci.: Mater. Electron.*, 2019, **30**, 15880–15888.

39 V. Uvarov and I. Popov, Metrological characterization of X-ray diffraction methods at different acquisition geometries for determination of crystallite size in nano-scale materials, *Mater. Charact.*, 2013, **85**, 111–123.

40 A. W. Faridi, M. Imran, G. H. Tariq, S. Ullah, S. F. Noor, S. Ansar and F. Sher, Synthesis and characterization of high-efficiency halide perovskite nanomaterials for light-absorbing applications, *Ind. Eng. Chem. Res.*, 2022, **62**, 4494–4502.

41 K. I. John, A. A. Adenle, A. T. Adeleye, I. P. Onyia, C. Amune-Matthews and M. O. Omorogie, Unravelling the effect of crystal dislocation density and microstrain of titanium dioxide nanoparticles on tetracycline removal performance, *Chem. Phys. Lett.*, 2021, **776**, 138725.

42 S. S. Hegde, P. Murahari, B. J. Fernandes, R. Venkatesh and K. Ramesh, Synthesis, thermal stability and structural transition of cubic SnS nanoparticles, *J. Alloys Compd.*, 2020, **820**, 153116.

43 E. Sarica, Investigation of spray pyrolyzed cubic structured Cu doped SnS films, *Phosphorus, Sulfur Silicon Relat. Elem.*, 2021, **196**, 1103–1108.

44 S. Rodríguez-Castro, C. Álvarez-Macías, M. Rivero, L. Salgado-Conrado, R. Loera-Palomo, B. Reyes-Durán and J. Narro-Ríos, Evaluation of SnS: Cu thin film properties obtained by USP technique to implement it as an absorbent layer in solar cells using SCAPS, *Coatings*, 2021, **11**, 754.

45 B. H. Baby and D. Bharathi, Mohan, Structural, optical and electrical studies of DC-RF magnetron co-sputtered Cu, In & Ag doped SnS thin films for photovoltaic applications, *Sol. Energy*, 2019, **194**, 61–73.

46 O. G. Abdullah, S. B. Aziz, K. M. Omer and Y. M. Salih, Reducing the optical band gap of polyvinyl alcohol (PVA) based nanocomposite, *J. Mater. Sci.: Mater. Electron.*, 2015, **26**, 5303–5309.

47 S. Zhang and S. Cheng, Thermally evaporated SnS: Cu thin films for solar cells, *Micro Nano Lett.*, 2011, **6**, 559–562.

48 V. R. Minnam Reddy, M. R. Pallavolu, P. R. Guddeti, S. Gedi, K. K. Yarragudi Bathal Reddy, B. Pejjai, W. K. Kim, T. R. R. Kotte and C. Park, Review on Cu2SnS3, Cu3SnS4, and Cu4SnS4 thin films and their photovoltaic performance, *J. Ind. Eng. Chem.*, 2019, **76**, 39–74.

49 P. S. Shewale and K.-S. Yun, Synthesis and characterization of Cu-doped ZnO/RGO nanocomposites for room-temperature H2S gas sensor, *J. Alloys Compd.*, 2020, **837**, 155527.

50 Y. Fu, F. Meng, M. B. Rowley, B. J. Thompson, M. J. Shearer, D. Ma, R. J. Hamers, J. C. Wright and S. Jin, Solution growth of single crystal methylammonium lead halide perovskite nanostructures for optoelectronic and photovoltaic applications, *J. Am. Chem. Soc.*, 2015, **137**, 5810–5818.

51 K. S. Gour, V. C. Karade, R. Parmar, J. S. Jang, S. Kazim, S. Jang, R. Gunnella, J. Park, J. H. Yun and J. H. Kim, In search of disorder transactions and defects within $Cu_2ZnSn(S,Se)_4$ based absorber layers *via* temperature-dependent Raman spectroscopy technique, *Sol. RRL*, 2023, **7**, 2200946.

52 A. T. Vicente, A. Araújo, M. J. Mendes, D. Nunes, M. J. Oliveira, O. Sanchez-Sobrado, M. P. Ferreira, H. Águas, E. Fortunato and R. Martins, Multifunctional cellulose-paper for light harvesting and smart sensing applications, *J. Mater. Chem. C*, 2018, **6**, 3143–3181.

53 H. Zhao, X. Xu, C. Li, R. Tian, R. Zhang, R. Huang, Y. Lyu, D. Li, X. Hu and L. Pan, Cobalt-doping in Cu_2SnS_3: enhanced thermoelectric performance by synergy of phase transition and band structure modification, *J. Mater. Chem. A*, 2017, **5**, 23267–23275.

54 B. H. Baby, A. M. Thomas, E. G. Amrutha and D. B. Mohan, Enhancement of optoelectronic properties *via* substitutional doping of Cu, in and Ag in SnS nanorods for thin film photovoltaics, *Sol. Energy*, 2020, **205**, 446–455.

55 P. R. Bommireddy, C. S. Musalikunta, C. Uppala and S.-H. Park, Influence of Cu doping on physical properties of sol-gel processed SnS thin films, *Mater. Sci. Semicond. Process.*, 2017, **71**, 139–144.

56 G. Sai Gautam, T. P. Senftle and E. A. Carter, Understanding the effects of Cd and Ag doping in Cu2ZnSnS4 solar cells, *Chem. Mater.*, 2018, **30**, 4543–4555.

57 M. Patel and A. Ray, Magnetron sputtered Cu doped SnS thin films for improved photoelectrochemical and heterojunction solar cells, *RSC Adv.*, 2014, **4**, 39343–39350.

58 A. S. Najm, H. S. Naeem, K. O. Alabboodi, S. A. Hasbullah, H. A. Hasan, A. M. Holi, A. A. Al-Zahrani, K. Sopian, B. Bais and H. S. Majdi, New systematic study approach of green synthesis CdS thin film *via* Salvia dye, *Sci. Rep.*, 2022, **12**, 12521.

59 D. Alagarasan, S. Varadharajaperumal, K. D. A. Kumar, R. Naik, S. Umrao, M. Shkir, S. AIFaify and R. Ganesan, Influence of nanostructured SnS thin films for visible light photo detection, *Opt. Mater.*, 2021, **121**, 111489.

60 A. Antony, P. Poornesh, I. V. Kityk, K. Ozga, J. Jedryka, P. Rakus and A. Wojciehcowski, X-ray photoelectron spectroscopy, Raman and photoluminescence studies on formation of defects in Cu: ZnO thin films and its role in nonlinear optical features, *Laser Phys.*, 2018, **28**, 95405.

61 N. R. Mathews, E. R. Morales, M. A. Cortés-Jacome and J. A. T. Antonio, TiO_2 thin films–Influence of annealing temperature on structural, optical and photocatalytic properties, *Sol. Energy*, 2009, **83**, 1499–1508.

62 P. Jain and P. Arun, Influence of grain size on the band-gap of annealed SnS thin films, *Thin Solid Films*, 2013, **548**, 241–246.

63 P. R. Bommireddy, C. S. Musalikunta, C. Uppala and S. H. Park, Influence of Cu doping on physical properties of sol-gel processed SnS thin films, *Mater. Sci. Semicond. Process.*, 2017, **71**, 139–144.

64 B. W. H. Baugher, H. O. H. Churchill, Y. Yang and P. Jarillo-Herrero, Optoelectronic devices based on electrically tunable p–n diodes in a monolayer dichalcogenide, *Nat. Nanotechnol.*, 2014, **9**, 262–267.

65 J. Guan, Z. Zhang, M. Dou, J. Ji, Y. Song, J. Liu, Z. Li and F. Wang, Thermoelectric properties of Bi-doped SnS: First-principle study, *J. Phys. Chem. Solids*, 2020, **137**, 109182.

66 T. Garmim, S. Chahib, L. Soussi, R. Mghaiouini, Z. El Jouad, A. Louardi, O. Karzazi, M. El Jouad, E. K. Hlil and B. Hartiti, Optical, electrical and electronic properties of SnS thin films deposited by sol gel spin coating technique for photovoltaic applications, *J. Mater. Sci.: Mater. Electron.*, 2020, **31**, 20730–20741.

67 S. Sebastian, I. Kulandaisamy, S. Valanarasu, M. Shkir, V. Ganesh, I. S. Yahia, H.-S. Kim and D. Vikraman, Physical and electrical properties' evaluation of SnS: Cu thin films, *Surf. Eng.*, 2021, **37**, 137–147.

68 S. Lavanya, T. R. Kumar, A. V. Juliet, J. Hakami, I. M. Ashraf and M. Shkir, Noticeable photo-sensing properties of SnS: Cu thin films fabricated by thermal evaporation technique, *Solid State Sci.*, 2022, **128**, 106889.

69 S. Sebastian, I. Kulandaisamy, A. M. S. Arulanantham, S. Valanarasu, A. Kathalingam, A. Jesu Jebathew, M. Shkir and M. Karunakaran, Influence of Al doping concentration on the opto-electronic chattels of SnS thin films readied by NSP, *Opt. Quantum Electron.*, 2019, **51**, 1–16.

70 A. Chaves, J. G. Azadani, H. Alsalman, D. R. Da Costa, R. Frisenda, A. J. Chaves, S. H. Song, Y. D. Kim, D. He and J. Zhou, Bandgap engineering of two-dimensional semiconductor materials, *npj 2D Mater. Appl.*, 2020, **4**, 29.

71 W. Zhou, G. Cao, M. Yuan, S. Zhong, Y. Wang, X. Liu, D. Cao, W. Peng, J. Liu and G. Wang, Core–shell engineering of conductive fillers toward enhanced dielectric properties: a universal polarization mechanism in polymer conductor composites, *Adv. Mater.*, 2023, **35**, 2207829.

72 H. Wu, H. L. Tan, C. Y. Toe, J. Scott, L. Wang, R. Amal and Y. H. Ng, Photocatalytic and photoelectrochemical systems: similarities and differences, *Adv. Mater.*, 2020, **32**, 1904717.

73 G. Larramona, S. Levcenko, S. Bourdais, A. Jacob, C. Choné, B. Delatouche, C. Moisan, J. Just, T. Unold and G. Dennler, Fine-tuning the Sn content in CZTSSe thin films to achieve 10.8% solar cell efficiency from spray-deposited water–ethanol-based colloidal inks, *Adv. Energy Mater.*, 2015, **5**, 1501404.

